PAPER

L-mode plasmas analyses and current ramp-up predictions for a JT-60SA hybrid scenario

IOP Publishing Plasma Physics and Controlled Fusion
Plasma Phys. Control. Fusion **63** (2021) 025014 (16pp) https://doi.org/10.1088/1361-6587/abcba9

L-mode plasmas analyses and current ramp-up predictions for a JT-60SA hybrid scenario

J Morales[1], J Garcia[1], G Giruzzi[1], J-F Artaud[1], C Piron[2], M Vallar[3], T Goodman[3] and JET[4] and MST1 contributors[5]

[1] CEA, IRFM, F-13108 Saint-Paul-lez-Durance, France
[2] ENEA, Fusion and Nuclear Safety Department, Frascati, Italy
[3] EPFL, SPC, Lausanne, Switzerland

E-mail: jorge.morales@cea.fr

Received 20 August 2020, revised 4 November 2020
Accepted for publication 18 November 2020
Published 23 December 2020

Abstract

In this work, L-mode analyses are performed in order to assess a modeling framework for the prediction of electron cyclotron resonant heating (ECRH) -assisted current ramp-up phases for JT-60SA tokamak hybrid scenario #4-2. We compare two turbulence transport models, CDBM and TGLF, using the integrated modeling code CRONOS. Model validation is performed on the basis of an L-mode ramp-up phase in a JET plasma, and a flat-top L-mode TCV (Tokamak a configuration variable) plasma with applied ECRH. Parameter scans in Z_{eff} and in-edge electron temperature (T_e) are performed. Our results indicate effective prediction of the q profile in JET ramp-up if edge T_e is properly captured. Indeed, our sensitivity scan demonstrates the strong impact of edge T_e on q profile evolution. The results of CDBM and TGLF modeling show good agreement with the experimental measurements. With respect to a JT-60SA hybrid scenario, a significant amount of ECRH *off-axis* is required to maintain a q profile above unity across the entire plasma radius. Based on an analysis of power deposition location, we find that ECRH applied close to $\rho = 0.33$ allows a compromise between a q profile larger than unity, and high central T_e. We evaluate two current ramp-up rates, where the fast rate is double that of the slower rate. The quantity of ECRH required for the fast ramp scenario is found to be greater by almost a factor of two than that required in the slow ramp scenario.

Keywords: integrated modeling, current ramp-up, safety factor control, hybrid tokamak scenario

(Some figures may appear in colour only in the online journal)

1. Introduction

The prediction of plasma performance essential in terms of assessing the potential development of present-day tokamaks, as well as in relation to future devices such as JT-60SA or ITER. In particular, predictions for the ramp-up phase are of special importance, as successful plasmas in the flat-top phase critically depend on the initial configuration. This is particularly the case for the so-called advanced scenarios, in which considerations such as plasma shape, flux consumption reduction, or the control of the q profile during ramp-up are mandatory [1–3]. To tackle these challenges, ECRH is an important resource used in present day tokamaks. However, the prediction and simulation of plasma behavior during ramp-up is a complex activity, due to a combination of several challenges: for instance, an accurate prediction of transport close to the separatrix, and of neoclassical resistivity, to achieve a precise computation of q profiles. Therefore, a reliable computation of the turbulent transport and current diffusion in L-mode

[4] See the author list of E Joffrin *et al* Nucl. Fusion 59, 112021 (2019).
[5] See the author list of H Meyer *et al* Nucl. Fusion 57, 102014 (2017).

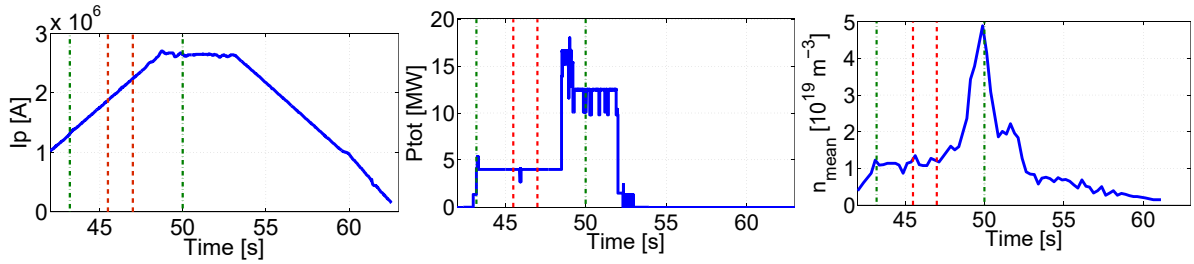

Figure 1. Characteristics of JET shot 72516: (left) plasma current, (center) total injected power and (right) average density. Vertical green lines indicate interpretative simulation intervals, vertical red lines indicate predictive simulation intervals.

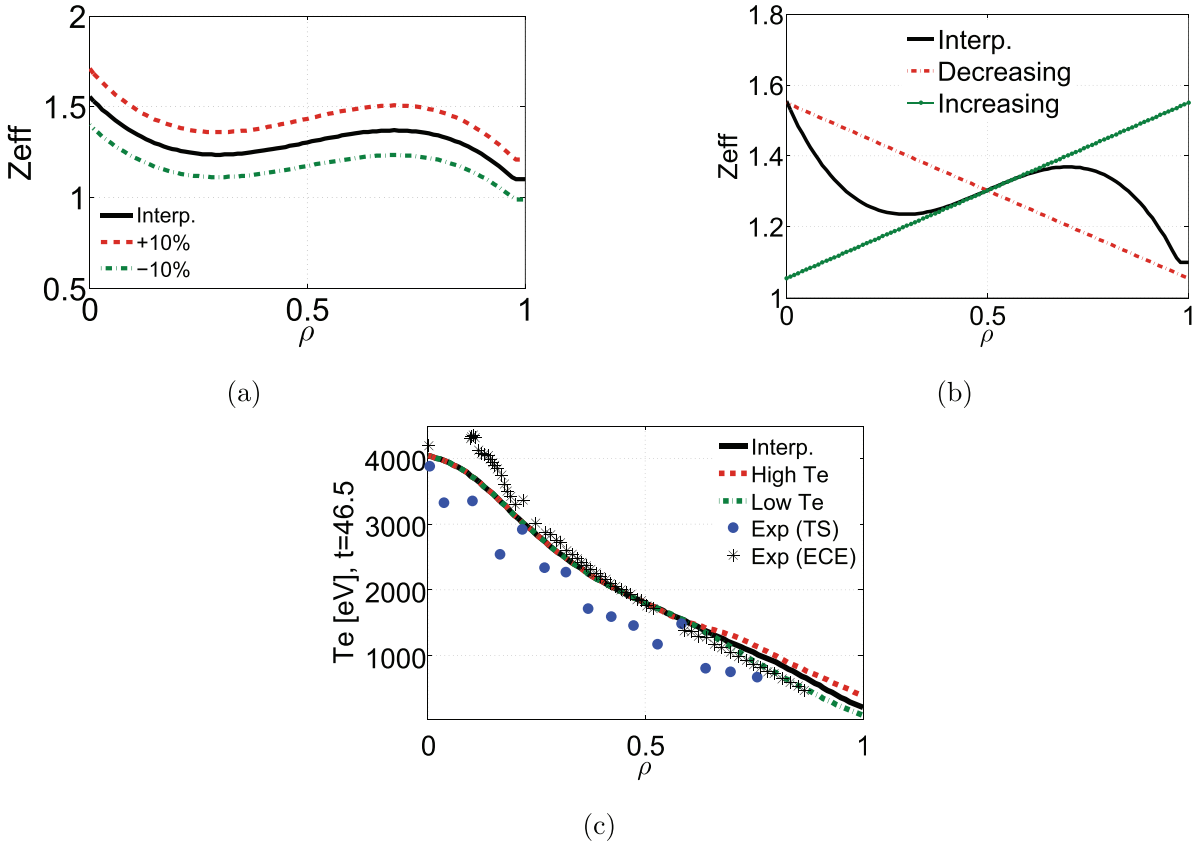

Figure 2. JET: illustration of different Z_{eff} profiles (a), (b) and electron temperature profiles (c) considered for the purpose of sensitivity analysis. In (c) we observe also the T_e profiles measured based on Thomson scattering (TS), and electron cyclotron emission (ECE) diagnostics. The three T_e profiles considered in the interpretative simulations are designated 'Interp.', 'High Te', and 'Low Te'.

is needed in order to accurately predict q profile evolution in ECRH assisted ramp-ups.

In this work, L-mode analyses are performed, combining plasmas from different tokamaks in order to assess and to provide a credible modeling framework for predictions of the ramp-up phase of JT-60SA, and the initial phase of ITER, for which ECRH is planned to be used [4–7]. In order to evaluate their predictive capabilities, we compare two turbulent transport models, CDBM [6, 8–10] and TGLF [11], using the integrated modeling code CRONOS [12]. To this end, we run simulations of the L-mode ramp-up phase inJET plasma, and in flat-top L-mode TCV plasma with applied ECRH. Parameter scans in relation to Z_{eff} and in the edge electron temperature (within the range of experimental uncertainties) are performed in order to assess the simulation's sensitivity to these quantities. Thevalidated model is then applied to JT-60SA ramp-up studies. We investigate the hybrid scenario #4-2 ramp-up [13]. The objective of this scenario is to achieve a safety factor (q) profile which is flat, close, and just above unity in order to avoid large sawteeth. Core plasma confinement is thereby improved, and long pulse sustainment is facilitated. In this scenario, the transition from L to H mode is expected to occur when neutral beam injection (NBI) is applied to the latter-half of the current ramp. In this study, we assess the evolution of the q profile from the onset of plasma formation until the moment prior to L-H transition. The objective is to estimate the ECRH level and the radial location of ECRH deposition required to obtain a q profile above unity. In an L-mode current ramp-up ECRH assistance is important, because in this phase electron temperature is low and the current diffusion

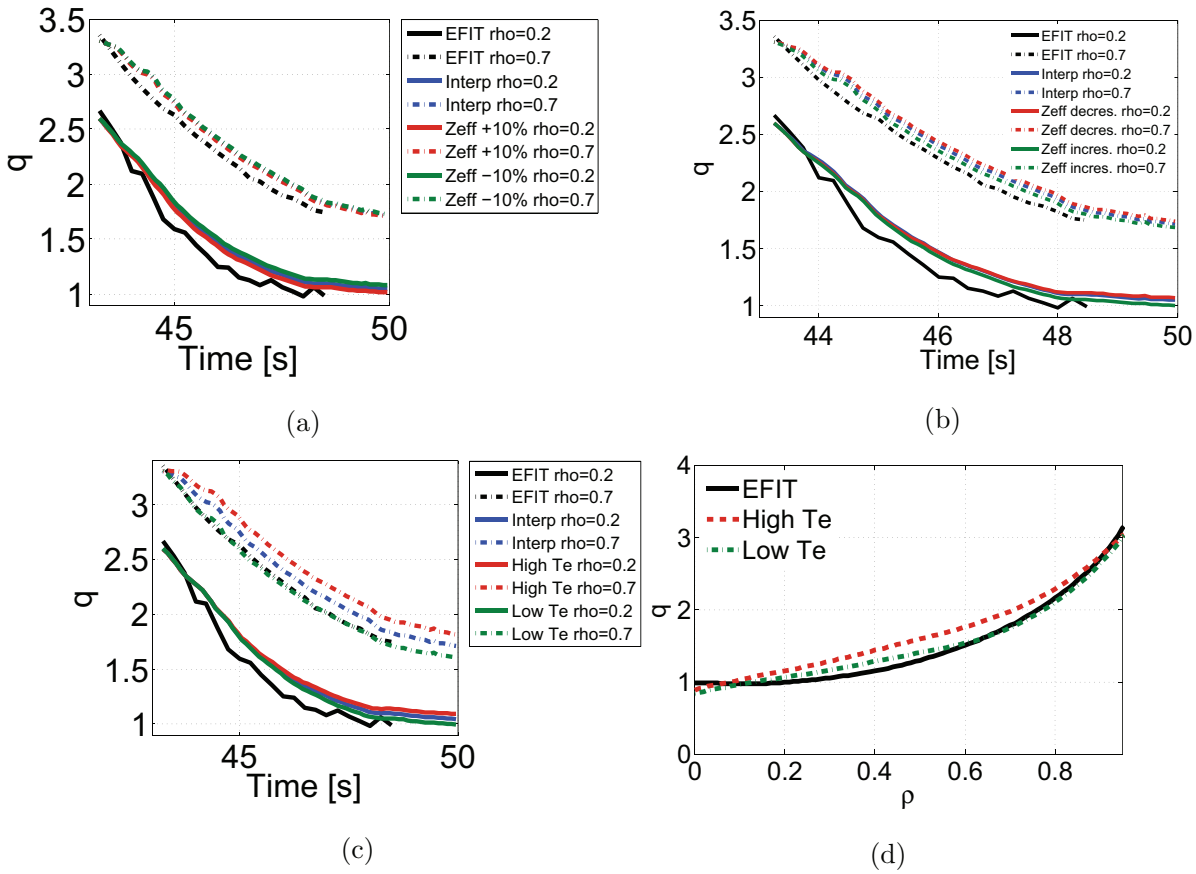

Figure 3. JET: q profile values as a function of time at $\rho = 0.2$ and $\rho = 0.7$: (a) effect of Z_{eff} profiles (same shape but $\pm 10\%$, see figure 2 (a)), (b) effect of Z_{eff} profiles (shape changed, see figure 2(b)) and (c) effect of edge T_e variations (see figure 2(c)). Here, the effect of T_e changes is more significant, particularly at $\rho = 0.7$. (d), q profile at $t = 48.485$ s.

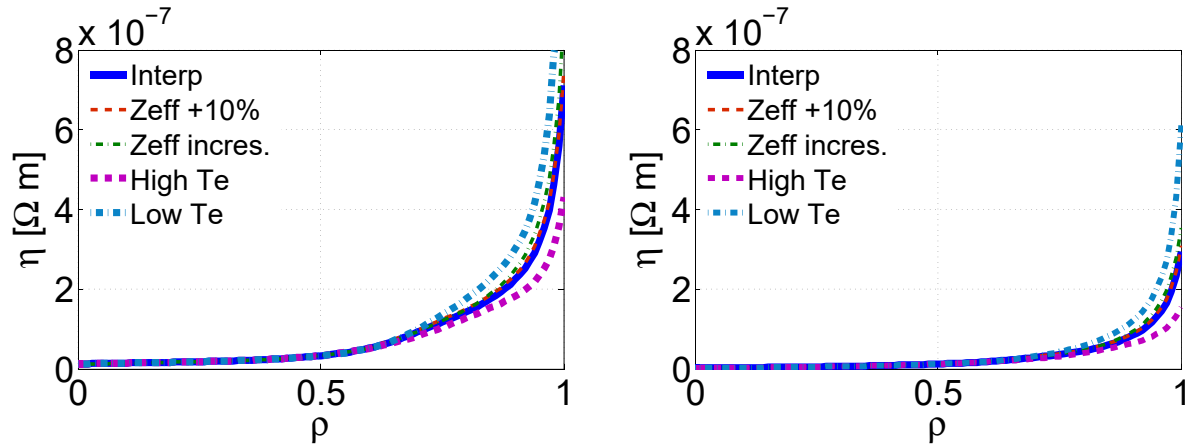

Figure 4. JET: neoclassical resistivity profile at $t = 44$ s (left) and $t = 49$ s (right) for different profiles of Z_{eff} and T_e (see figure 2).

fast, causing the central safety factor value to decrease. To prevent the central q value being smaller than unity, and to achieve a hybrid scenario, EC heating and current drive are both needed. To tackle this problem, in this paper, the ECRH power required is assessed on the basis of a JT-60SA hybrid #4-2 scenario.

This paper is organized as follows: in section 2 we show the performed validation of neoclassical resistivity and turbulence models using JET ramp-up experimental data. In section 3 we validate the ECRH ray tracing and power deposition model using TCV experimental data. In section 4, we use the validated model to estimate the ECRH power level and location enabling the q profile to be larger than unity in JT-60SA hybrid #4-2 scenario. For this scenario two different current ramp-up rates are compared. Our conclusions are presented in section 5.

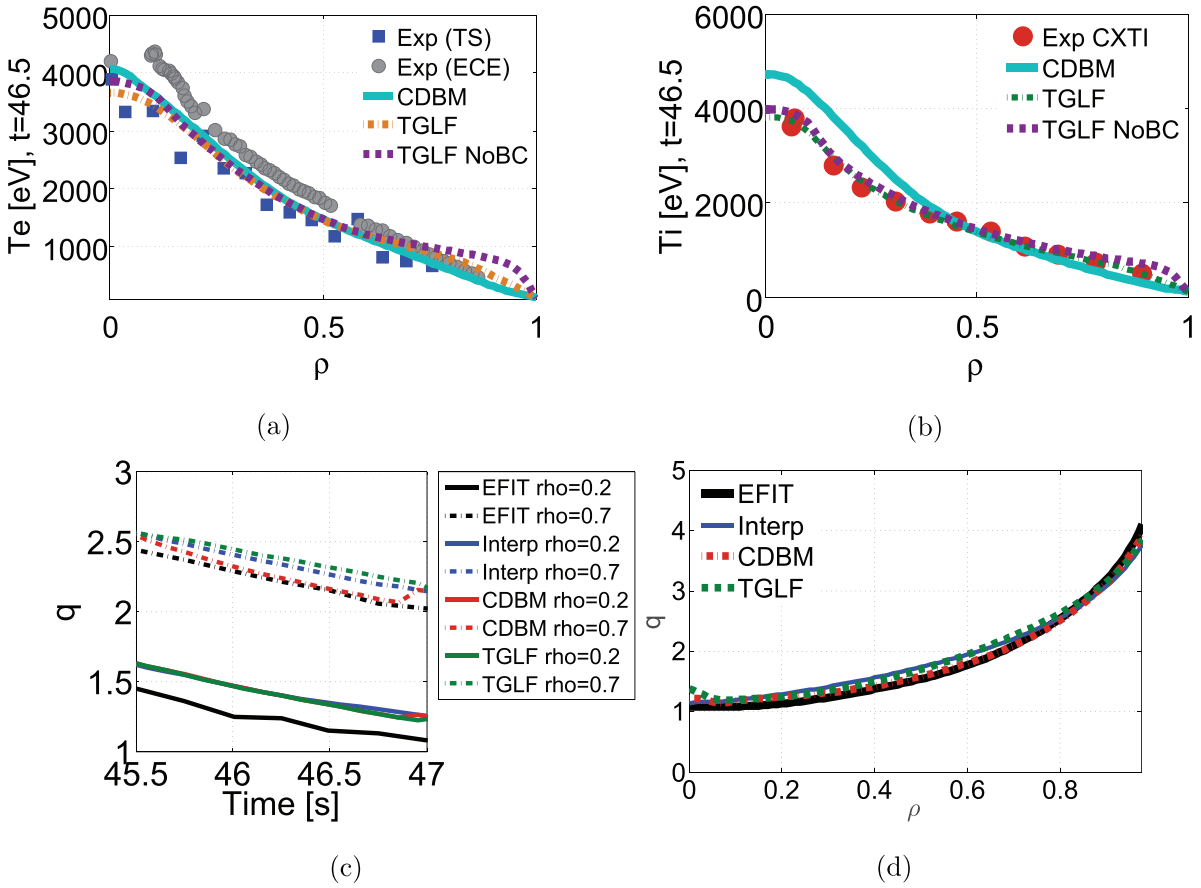

Figure 5. JET: (a) predicted T_e for CDBM and TGLF models compared to experimental measurements based on Thomson scattering (TS) and electron cyclotron emission (ECE) diagnostics. With respect to TGLF NoBC, the acronym means that the model is used up to $\rho = 1$, otherwise the model prediction stops at $\rho = 0.9$. (b) Predicted T_i compared to experimental measurements performed via the charge exchange (CX) diagnostic. (c) Predicted q profile evolution for CDBM and TGLF models compared to EFIT q profile reconstruction. (d) q profiles at $t = 46.8$ s.

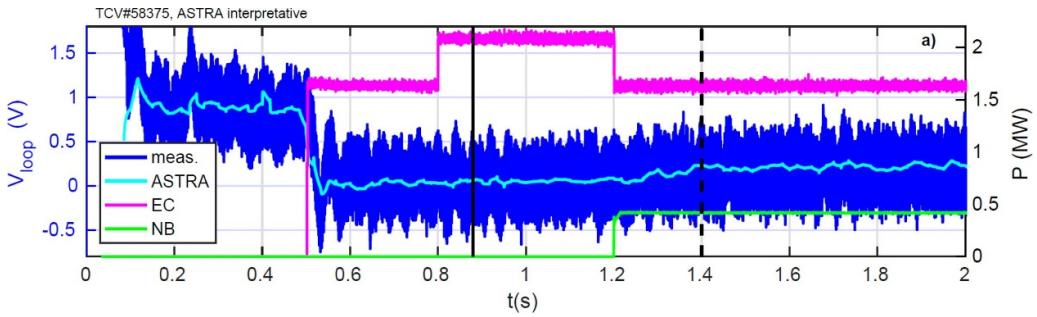

Figure 6. TCV pulse 58 375. V_{loop} evolution (both measured and via the ASTRA [22] interpretative simulation). Electron cyclotron (EC) and neutral beam (NB) waveforms. Solid vertical line corresponds to $t = 0.88$ s and dashed vertical line to $t = 1.40$ s.

2. Neoclassical resistivity and turbulence model validation

In our sensitivity study we vary the Z_{eff} profile and edge electron temperature. The Z_{eff} profile measures the plasma composition, and is defined as

$$Z_{\text{eff}}(\rho) = \sum_i \frac{n_i(\rho) Z_i^2}{n_e(\rho)}, \qquad (1)$$

with Z_i as the i ion atomic number, $n_i(\rho)$ as the i ion density profile and $n_e(\rho)$ denoting the electron density profile. As radial coordinate we consider $\rho = \sqrt{\Phi/\Phi_{sep}}$, the normalized toroidal flux coordinate. We then analyze the current ramp-up of the JET 72 516 pulse. This shot is selected due to the availability of motional Stark effect (MSE) constrained equilibrium reconstruction via EFIT [14]; in this way, the accuracy of the q profile reconstruction, particularly at the plasma core, is improved. In figure 1, the time evolution of the plasma current (I_p), total injected power (P_{tot}), and mean electron density

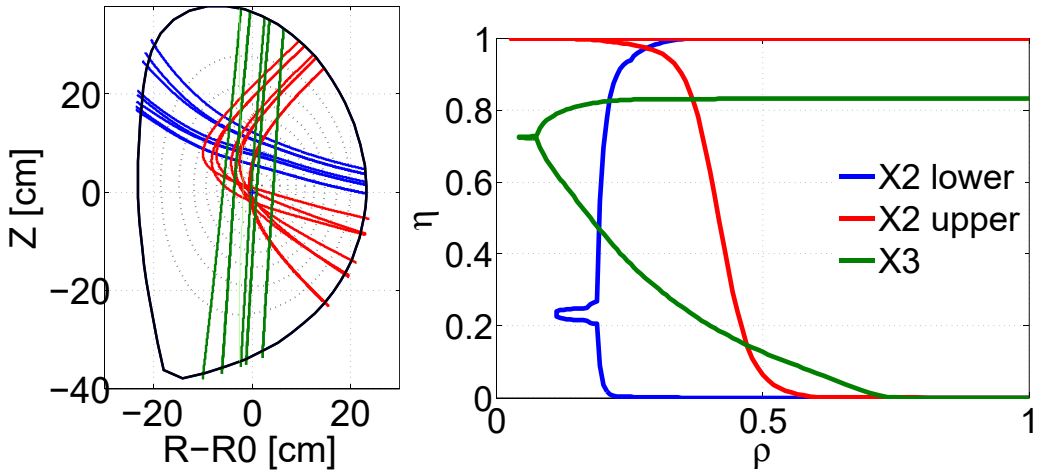

Figure 7. TCV: (left) EC wave ray tracing, using two X2 EC launchers at the low field side in upper and lower locations, together with one X3 launcher at the top. (Right) absorption ratio as a function of plasma radius ρ.

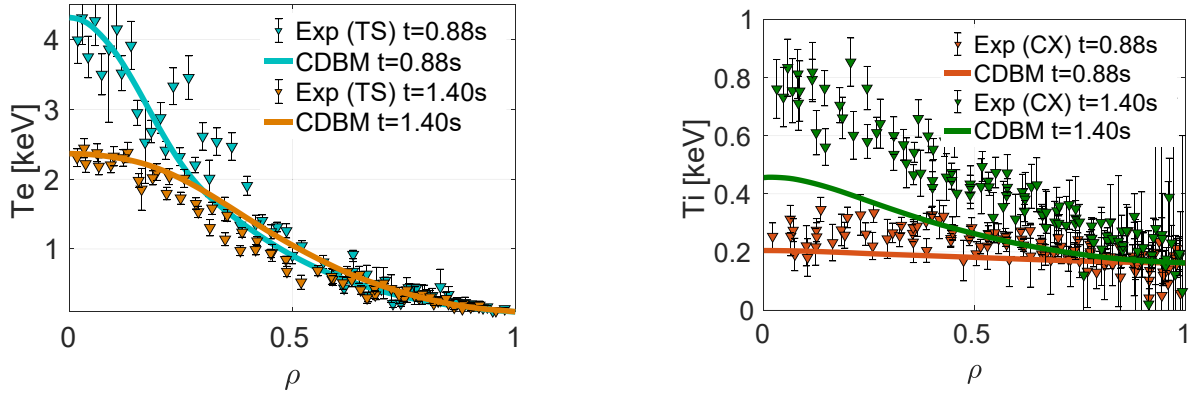

Figure 8. TCV: comparison of (left) T_e profiles from Thomson scattering (TS) diagnostic, (right) T_i profiles from charge exchange (CX) diagnostic.

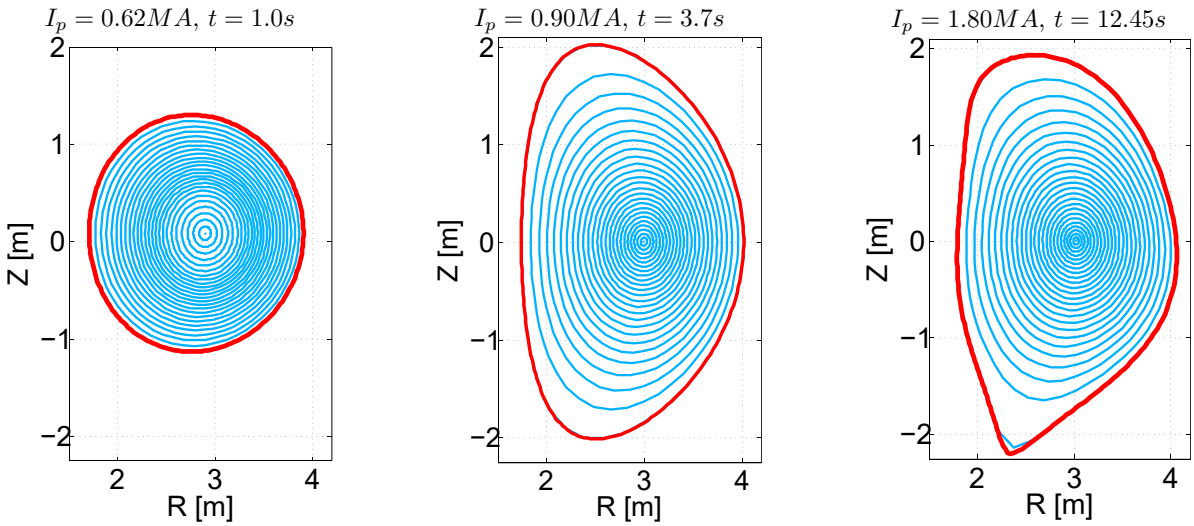

Figure 9. JT-60SA : equilibrium evolution for scenario #4-2 ramp-up. L-H transition occurs just after $t = 12.45$ s. The L-H transition power threshold is estimated at 4.9 MW (see figure 21 left).

(n_{mean}) are presented. The total injected power is composed of around 3 MW of NBI and 1 MW of ohmic power between $t = 43.26$ s and $t = 48.51$ s.

Interpretative simulations are performed for the sensitivity study: interpretative means that only the current diffusion equation, together with Grad–Shafranov equation, are

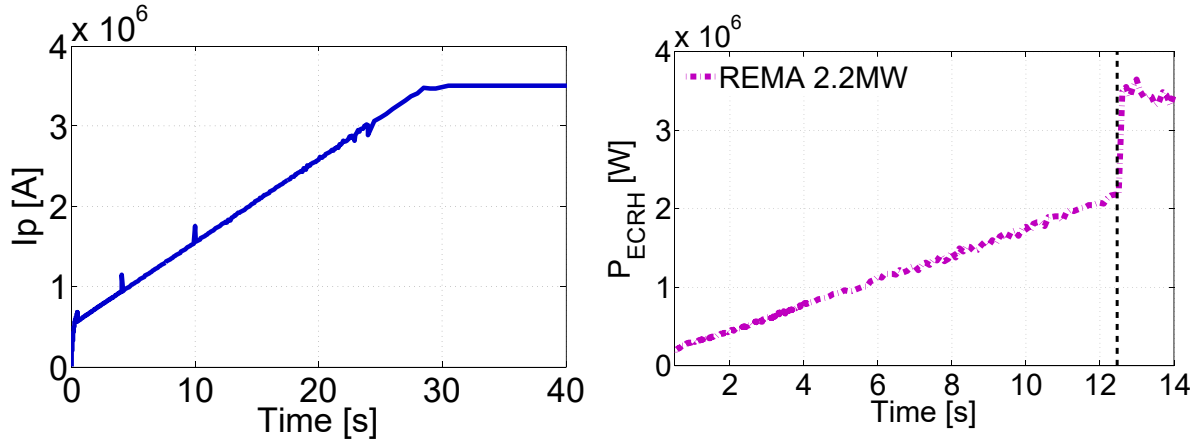

Figure 10. JT-60SA: (left) *Ip* ramp-up, (right) EC power.

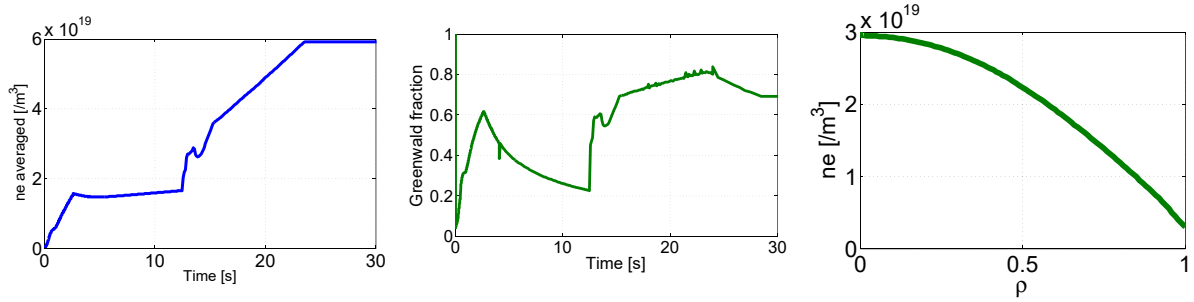

Figure 11. JT-60SA: (left) averaged electron density evolution, (center) Greenwald fraction, and (right) electron density profile at $t = 12.45$ s.

considered [12]. This equation is solved using NCLASS [15] for the computation of neoclassical resistivity. We take into account a plasma composed mainly of deuterium, with 5% hydrogen and 1% carbon content. The time interval considered is from $t = 43$ s to $t = 50$ s (see vertical dash-dotted green lines in figure 1). Five time-constant Z_{eff} profiles are tested, from which we take the measured value, $\pm 10\%$ of the profile, and decreasing and increasing linear functions (see figures 2(a) and (b)). With respect to the edge electron temperature, we consider a variation of $\pm 15\%$ at $\rho = 0.8$ (figure 2(c)). The T_e profiles are taken from experimental measurements, and therefore evolve over time. The impact of these changes are illustrated in figure 3. In this figure we observe that variations in Z_{eff} have only a weak effect on safety factor evolution. Both a $\pm 10\%$ alteration, and the change of profile shape only modify the final q values by a few percent. These results are in agreement with those of a previous publication [16]. On the other hand, a larger effect is observed in terms of edge T_e variation on q profile evolution. If we decrease the edge T_e by 15% (within experimental uncertainties) we are able to match the EFIT reconstructed values (we obtain a q profile change at $\rho = 0.7$ of more than 10%). Figures 3(c) and (d) show that if we consider a low edge T_{e}. the simulated q profile is closer to the EFIT equilibrium reconstruction.

The difference in terms of the impact of Z_{eff} and edge T_e on q can be explained by the stronger impact of edge T_e on neoclassical resistivity. In figure 4 this effect can be observed, the edge electron temperature variation induces a change in neoclassical resistivity of more than 10% at the plasma periphery. Low T_e values at the edge allow a better match with the experimental data, since neoclassical resistivity is large, and therefore current core penetration is faster, and q profile decreases at a stronger rate (see q profile in figure 3(c) and neoclassical resistivity in figure 4). In fact, resistivity multiplies the diffusive term on the current diffusion equation, causing the current to diffuse more rapidly towards the plasma center (see equation (1) in [12]).

Predictive simulations (evolving the flux function ψ, T_e, and T_i) are performed to evaluate the precision of the turbulence models. The time interval considered for these simulations is $t = [45.5\text{ s}, 47\text{ s}]$ (see vertical dashed red lines in figure 1). The initial condition is the interpretative simulation, 'Interp.' presented in the previous section (see figures 2 and 3). In figures 5(a) and (b) the computed T_e and T_i profiles are compared at $t = 46.5$ s (two thirds of simulation interval) to the experimental T_e measured with Thomson scattering (TS) together with electron cyclotron emission diagnostic (ECE), and T_i measured with the charge exchange diagnostic (CX). The CDBM model produces a good prediction of T_e profile. With regard to the ion temperature profile, the edge plasma is well predicted; however, at the plasma center, T_i is overpredicted. This can be explained by the fact that CDBM computes a single diffusion coefficient for T_e and T_i. Further details regarding this limitation are given in

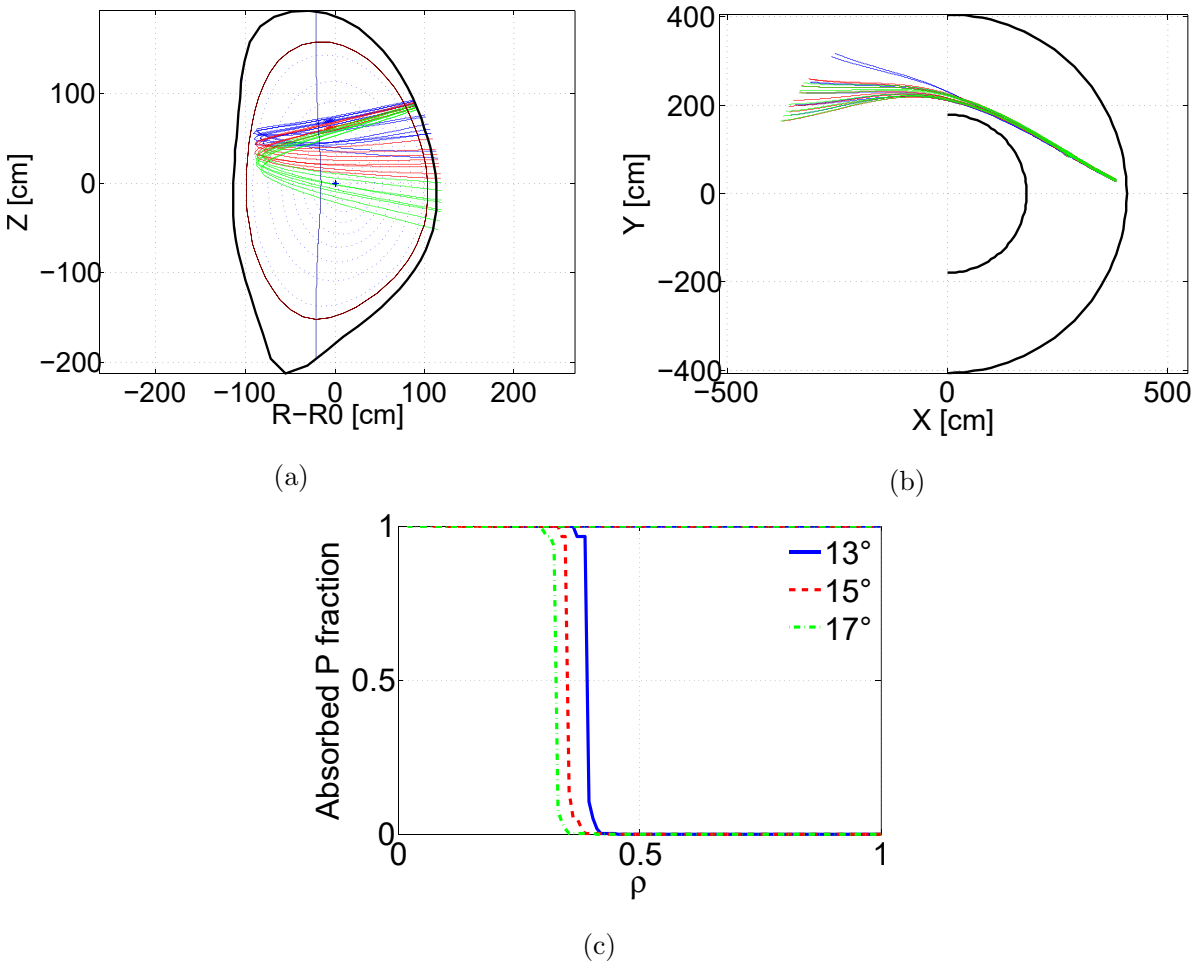

Figure 12. JT-60SA: (a) Poloidal view of ray trajectory. (b) Toroidal view of ray trajectory. (c) Absorbed power fraction. The three angles correspond to the poloidal injection angles of the EC beam (see appendix A.2 in [13]).

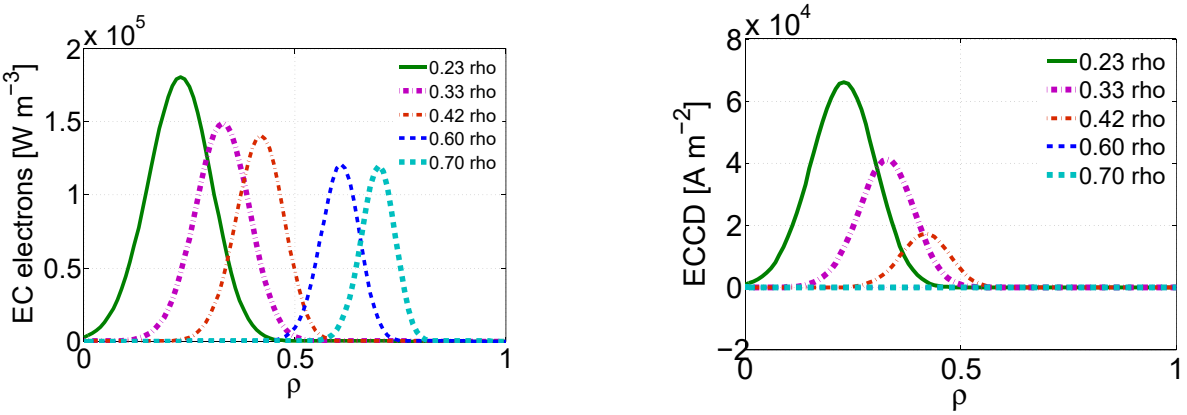

Figure 13. JT-60SA: (left) EC power deposition on electrons, (right) EC current density source, at $t = 12.45$ s (just before L-H transition) for injection poloidal angles varying from $-8°$ to $23°$ (see appendix A.2 in [13]). Here, we have a $25°$ toroidal injection angle, an EC frequency of 138 GHz, and a toroidal field of 2.28 T at a radius of 2.93 m.

section 3. TGLF with a boundary condition (BC) at $\rho = 0.9$ also provides a good prediction, but an artificial pedestal forms when the BC is at $\rho = 1$ (see NoBC profiles in figures 5(a) and (b)). This problem is known as *shortfall*, and arises owing to under-resolved GYRO radial computations (GYRO simulations are used to calibrate TGLF); this problem has recently been fixed [17], but the newly calibrated TGLF was not used in this study.

The accuracy of CDBM and TGLF are also verified when comparing the safety factor evolution with the EFIT reconstruction (figure 5(c)). In this figure, we observe that CDBM and TGLF computations reproduce q profile evolution at

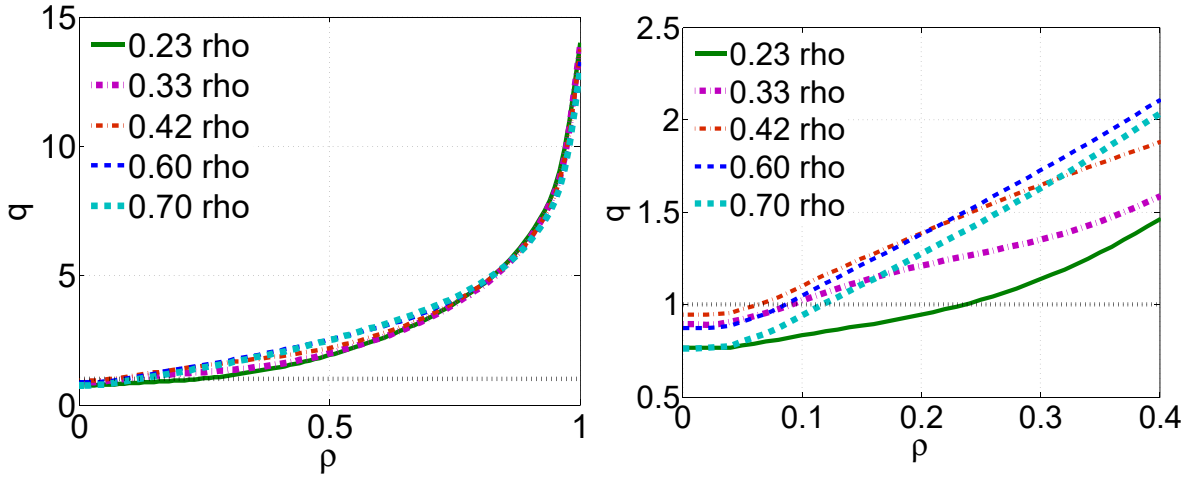

Figure 14. JT-60SA: (left) q profile at L-H transition, (right) core q profile at $t = 12.45$ s (just before L-H transition

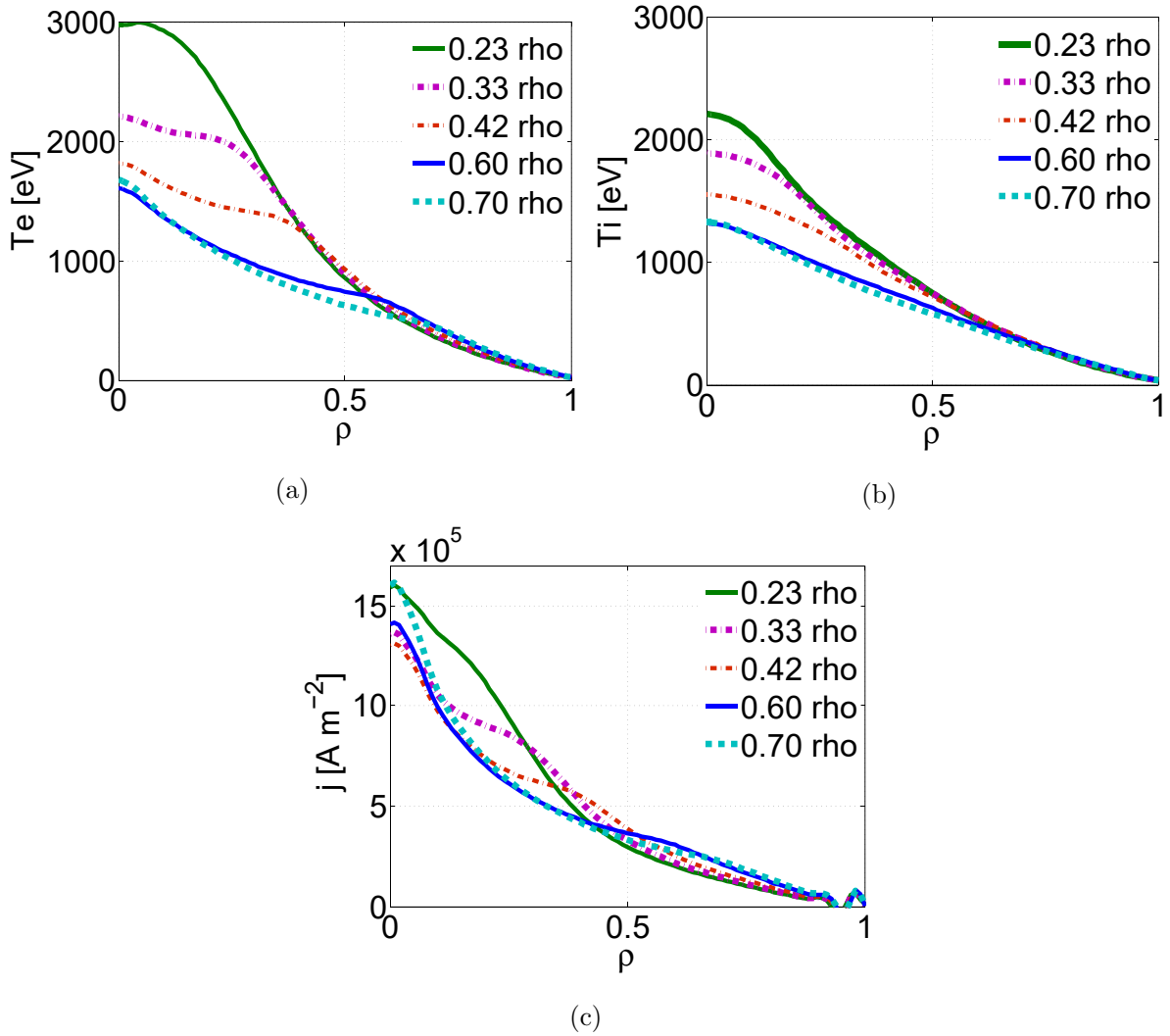

Figure 15. JT-60SA: (a) T_e profiles, (b) T_i profiles, (c) current density profiles at $t = 12.45$ s (just before L-H transition).

$\rho = 0.2$ and $\rho = 0.7$. As previously mentioned, to start the predictive simulation we use the interpretative run, 'Interp.'. For this reason, the starting point does not correspond to that of the EFIT equilibrium reconstruction. Looking at the q profile evolution, we note that the decay rate is similar for EFIT and for the two turbulence models. However for CDBM at $\rho = 0.7$,

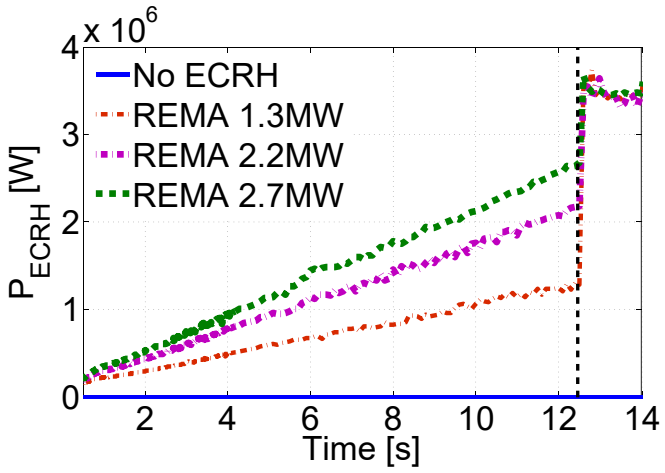

Figure 16. JT-60SA: EC power injected.

the decay rate is slightly faster. This effect is explained by the lower edge temperatures predicted by CDBM, as compared to the TGLF model (see figure 5(a)). With CDBM, therefore, the edge neoclassical resistivity is larger, the current diffusion is stronger, and the edge q profile decreases slightly faster. In figure 5(d) the q profiles computed by EFIT, interpretative, CDBM and TGLF simulations are compared. We find that the four profiles are in relatively good agreement.

All previous results allow us to validate the neoclassical resistivity calculation and both CDBM and TGLF turbulence transport models in CRONOS. In the following we use only CDBM. This model has two advantages compared to TGLF: firstly, it can be used up to $\rho = 1$ (no *shortfall* problem) and it has a faster computation time. In addition, the CDBM model has been successfully benchmarked against other turbulence models: see, for example [6, 10, 18]. In the next section we validate the ECRH source code REMA [19] using CDBM as our turbulence model.

3. ECRH source code validation

To validate the ray-tracing and ECRH deposition code REMA [19] integrated in CRONOS, we used experimental data from TCV. The L mode pulse selected here is number 58 375 (see figure 6). This is a lower single null discharge, where $I_p = 148$ kA, $B_{\text{tor}} = 1.43$ T, and mean electron density $n_{\text{mean}} = 1.5 \times 10^{19}$ m^{-3}. In order to validate REMA using the CDBM turbulence model, we take into account two instants on this pulse: at $t = 0.88$ s, where X2 (82.7 GHz) and X3 (117.8 GHz) EC waves are injected, and at $t = 1.40$ s, where we have X2 and NBI. The NBI source term is computed using NUBEAM [20, 21]. In figure 7 we show ray tracing of the EC waves and the absorption ratio at $t = 0.88$ s. Full absorption of X2, and 80% absorption of X3 are observed.

The comparison of experimental temperature profiles and predictive simulation with REMA and CDBM is presented in figure 8. Electron and ion temperature profiles are measured respectively with Thomson scattering (TS) and charge exchange (CX) diagnostics. The calculation is accurate for T_e, but T_i is underestimated. In fact, the CDBM model computes a single thermal diffusion coefficient applied to T_e and T_i. CDBM solves the transport coefficient for the pressure equation, where $P = n_e(T_e + T_i)$. Therefore if both temperatures are different (in this particular case $T_i \ll T_e$) the model is better able to predict the temperature profile with larger gradients (in this case, the T_e profile).

In this case, there is an important difference in the TCV pulse between ion and electron temperatures ($T_i/T_e < 0.4$). This fact makes CDBM underestimate T_i. To limit underpredictions of T_i using CDBM, as a safety check, we will verify that the ratio $T_i/T_e > 0.5$ in the remainder of this study. In addition, the next section examines the prediction of q profile evolution in ECRH assisted ramp-ups. Previous results have shown that T_e prediction via CDBM is correct and robust. For example, despite the fact that for TCV, T_i is underpredicted, T_e is well reproduced (see figure 8). As shown in the first section, T_e is the quantity with the stronger impact on neoclassical resistivity, and in consequence, on the q profile (the quantity of interest). Therefore, based on sections 2 and 3, we consider that a good modeling framework for q profile predictions with ECRH is to use a combination of REMA and CDBM. In the next section, we apply the modeling frameworks REMA and CDBM to current JT-60SA ramp-up studies.

4. Application to JT-60SA ramp-up prediction

Following the validation of the REMA and CDBM transport models, we apply CRONOS to the JT-60SA hybrid scenario #4-2 ramp-up [13]. The goal of this study is to determine the level and location of EC power, making the q profile larger than unity prior to L-H transition. In H mode, the q profile is almost frozen because the resistivity is low due to a high electron temperature. Therefore, if we reach L-H transition with the q profile above unity, a hybrid scenario without sawteeth can be more easily obtained.

In this section, we analyze two current ramp-ups: the first reaches a plateau at $t = 28$ s (slow Ip ramp); the second at $t = 15$ s (fast Ip ramp). With respect to the slow Ip ramp, we first analyze the effect of the radial power deposition location with fixed EC power. We then determine the level of EC power injected off-axis in order to achieve a q profile larger than unity. For the fast Ip ramp, we perform the same exercise to assess the amount of EC power needed to achieve a q profile above unity. Note that the current ramp-up rate is one of the main parameters used in order to optimize flux consumption, flat-top duration, the avoidance of MHD instabilities, etc. In all of the following simulations, we consider a plasma composed mainly of deuterium, with 5% hydrogen and 3% carbon. We begin by presenting the equilibrium evolution during the slow Ip ramp-up prior to L-H transition (see figure 9).

For the slow Ip ramp (figure 10 left) we test the effect of EC deposition location, taking into account a linear power ramp-up from 0.16 MW at $t = 0.5$ s to 2.2 MW at $t = 12.45$ s (see figure 10 right). Experimentally, the increase in EC power does not occur linearly, because the gyrotrons are turned on

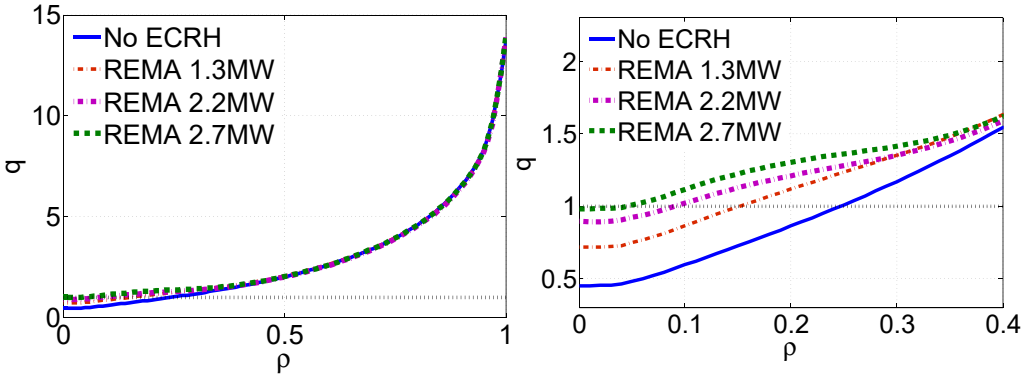

Figure 17. JT-60SA: (left) q profile at L-H transition, (right) core q profile at $t = 12.45$ s (just before L-H transition).

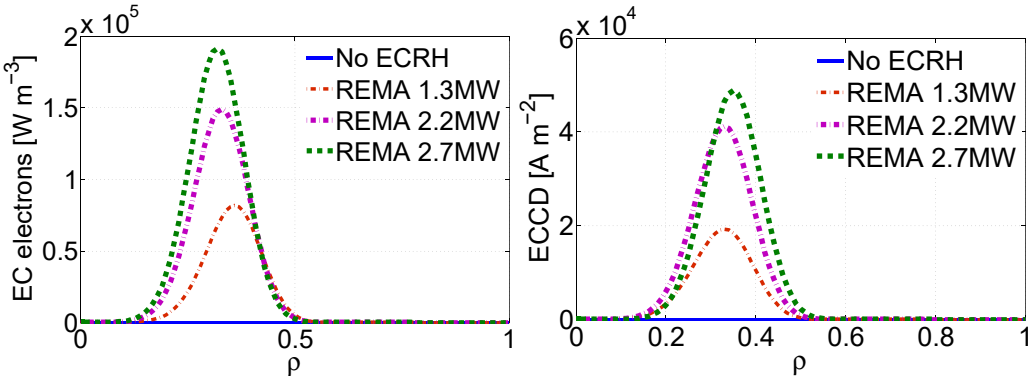

Figure 18. JT-60SA: (left) EC power deposition on electrons, (right) EC current density source at $t = 12.45$ s (just before L-H transition).

one by one; in our simulations, for simplicity, we consider a linear increase. To assess the impact of a more realistic EC power ramp, we compare linear and staircase ramps at the end of this section. For all cases, we consider the same density evolution (see figure 11). Notice that n_e averaged is almost constant between $t = 3$ s and $t = 12.45$ s (just before L-H transition). Therefore, between these two instants, the Greenwald fraction decreases because Ip is increasing (see figure 11 center).

For a power deposition close to $\rho = 0.33$, the wave ray tracing and absorbed power fraction at $t = 12.45$ s are illustrated in figure 12. In this figure we observe full absorption of EC power. We vary the deposition radius from $\rho = 0.23$ to $\rho = 0.7$ by varying the EC poloidal injection angle. The power and current source locations computed with REMA are shown in figure 13. We compute power deposition and current density source profiles discretising the wave beam in 113 rays, summing up their contributions, and smoothing the result with a Gaussian function. We find that with increasing radial position, the power and current sources decrease. Furthermore, the current source drops to very small values and becomes negligible for a deposition radius where $\rho > 0.5$ (see figure 13 right).

Figure 14 illustrates the effect of power deposition radius on q profile. At position $\rho = 0.5$, the safety factor value increases with increasing radial deposition (see figure 14 left). On the other hand, at the plasma core (figure 14 right), if the power deposition is in the range $\rho = (0.33, 0.6)$, the safety factor profile is high at the plasma center ($\rho \in (0, 0.3)$). If power is deposited at $\rho = 0.7$, the q profile is higher at $\rho = 0.5$ but it then drops faster towards the core. Based on these results, we conclude that to achieve a q profile higher than unity, particularly at the plasma's center, we need the deposited EC power to be between $\rho = 0.33$ and $\rho = 0.6$.

In figure 15 we present T_e, T_i, and the current density profile, defined as $j(\rho) = \langle R \rangle \langle \mathbf{j} \cdot \nabla \phi \rangle$ (with $\langle ... \rangle$ the average on a flux surface). In the figure, we note that the central T_e and T_i both drop with increasing deposition radius. Current density profile peaking decreases with power deposition radius, varying from $\rho = 0.23$ to $\rho = 0.40$, then increases again when power is deposited from $\rho = 0.60$ to $\rho = 0.70$. For large off-axis EC power deposition the temperature is low, and therefore resistivity is high, and the current is almost fully determined by the ohmic current, which in turn depends on the electron temperature through conductivity. Therefore, the peaking of the current will be determined primarily by the peaking of T_e. The peaking is high for extreme cases in the scan, whereas for intermediate cases there is a region of flat T_e in the core, which helps to flatten the current.

We need to find a compromise between large central T_e and a safety factor profile larger than unity. We conclude that, to obtain simultaneous high q profiles and high central T_e, a good compromise is to deposit EC power close to $\rho = 0.33$. We verify also that for all cases the ratio $T_i/T_e > 0.5$.

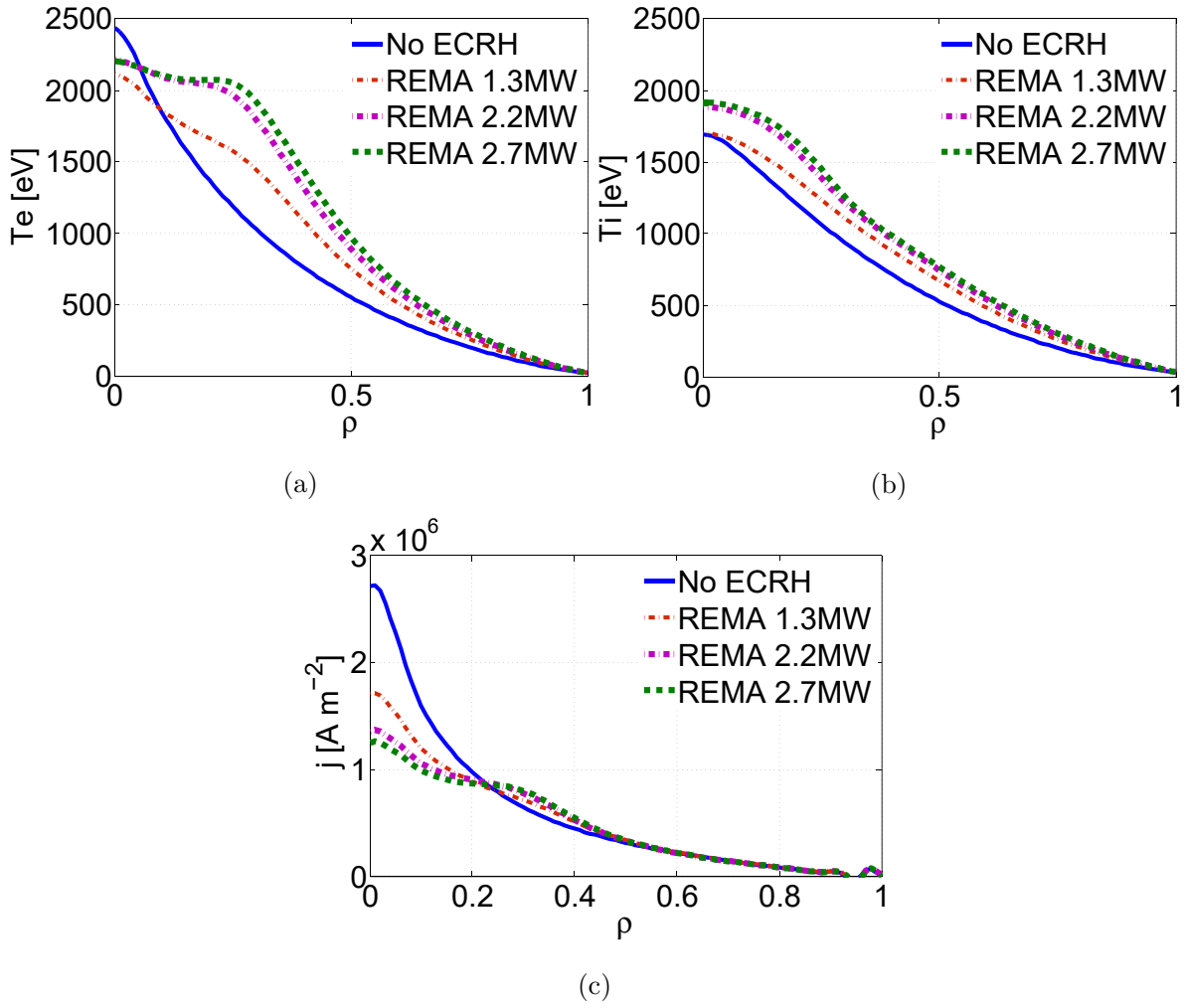

Figure 19. JT-60SA: (a) T_e profiles, (b) T_i profiles, (c) current density profiles at $t = 12.45$ s (just before L-H transition).

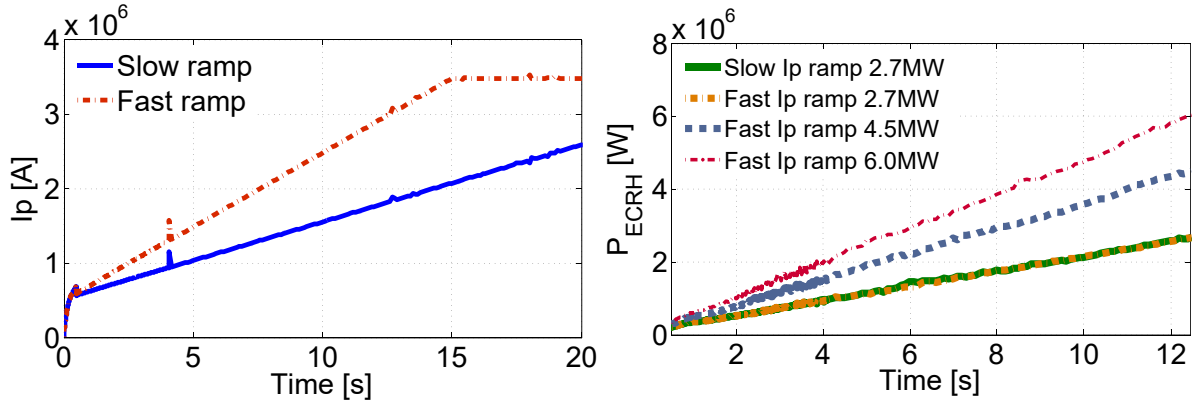

Figure 20. JT-60SA: (left) fast ramp considered in relation to previous slow current ramp, (right) ECRH power injected considered for fast and reference slow Ip ramp.

With a fixed power deposition radius at $\rho = 0.33$, in the next part of the study we vary the EC power levels. Injected EC power is increased linearly from a fixed value of 0.16 MW at $t = 0.5$ s to respectively 1.3, 2.2 and 2.7 MW at $t = 12.45$ s (see figure 16). Different runs are conducted until we are able to find a final EC power producing a q profile larger than unity. In figure 17 we observe the q profile at $t = 12.45$ s. With increasing EC power, the core q profile increases. At a maximum power of 2.7 MW, the q profile is above unity for all radii. The change in q profile is mainly visible for $\rho < 0.4$. As expected, the power and current drive are larger with injected EC power (see figure 18). The power and current drive

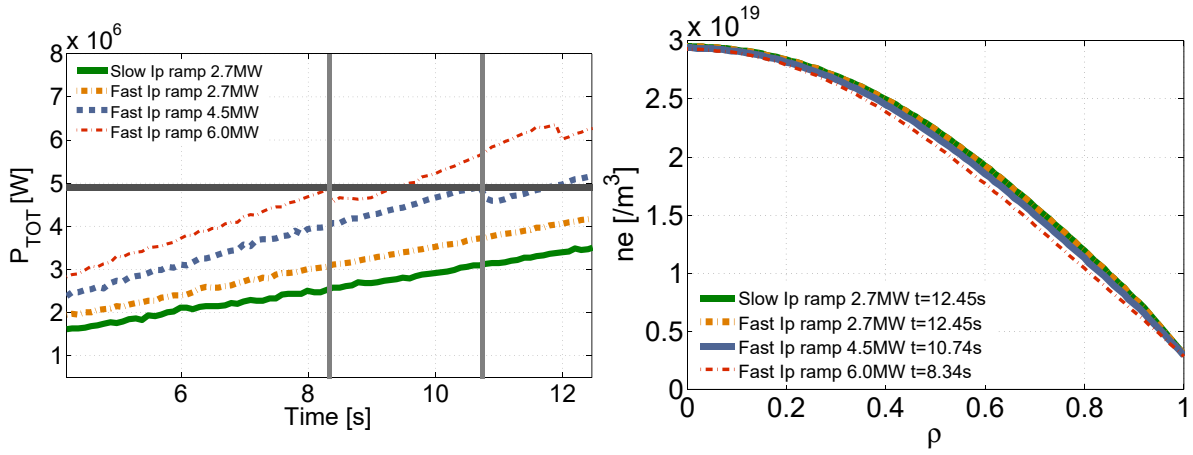

Figure 21. JT-60SA: (left) total power (ECRH plus ohmic) and L-H transition threshold (horizontal gray line), (right) electron density profile prior to L-H transition.

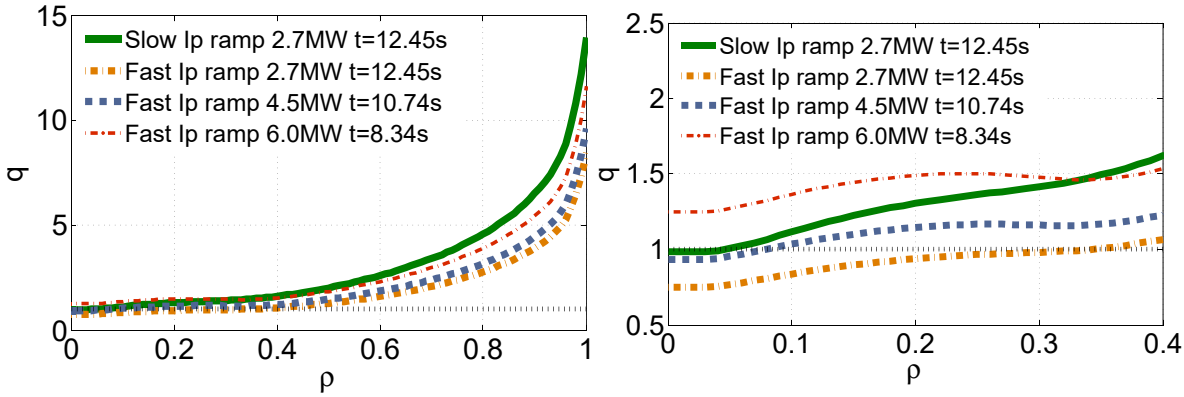

Figure 22. JT-60SA: (left) q profile, (right) zoom of q profile prior to L-H transition.

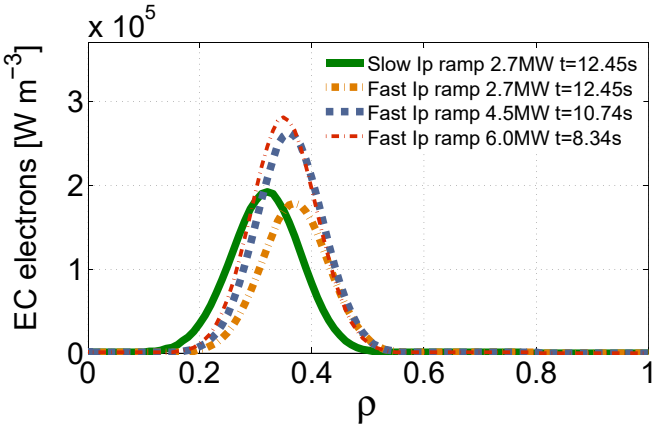

Figure 23. JT-60SA: EC power deposition on electrons.

deposition peak is not radially constant for all cases, because T_e profiles change due to the different levels of EC power. In figure 19, we observe the significant change in T_e and current density, j, with power. The T_e and j profiles flatten at the center where $\rho < 0.4$. In all cases, the temperature ratio found is $T_i/T_e > 0.5$. We conclude that to maintain a q profile above unity requires an EC power ramp finishing at a minimum of 2.7 MW (see figures 16 and 17), with a power deposition at $\rho = 0.33$.

For the fast *Ip* ramp (see figure 20 left) we obtain results similar to those for the slow *Ip* ramp. However, the ECRH power needed for q profile to be larger than unity is higher. As a consequence, the L-H transition occurs earlier for cases with high EC power injection. In figure 20 we show the two current ramps and the different ECRH power waveforms taken into account in the simulations. Injected powers vary from 0.16 MW at $t = 0.5$ s to 2.7 MW, 4.5 MW and 6.0 MW at $t = 12.45$ s. The time of L-H transition is not the same for all cases, because the EC power injected is higher, and EC power alone is able to trigger the L-H transition. In figure 21 (left) we observe the total power evolution, where the L-H power threshold is evaluated automatically in CRONOS at 4.9 MW using ITPA scaling [23]. For fast *Ip* ramp cases at 4.5 and 6.0 MW of ECRH, the L-H transition occurs at respectively $t = 10.74$ s and $t = 8.34$ s. In the following the profiles of interest are plotted at the time prior to L-H transition, i.e. at $t = 12.45$ s, except for the last two cases, where we plot the profiles at $t = 10.74$ s and $t = 8.34$ s. To begin, density profiles are plotted in figure 21

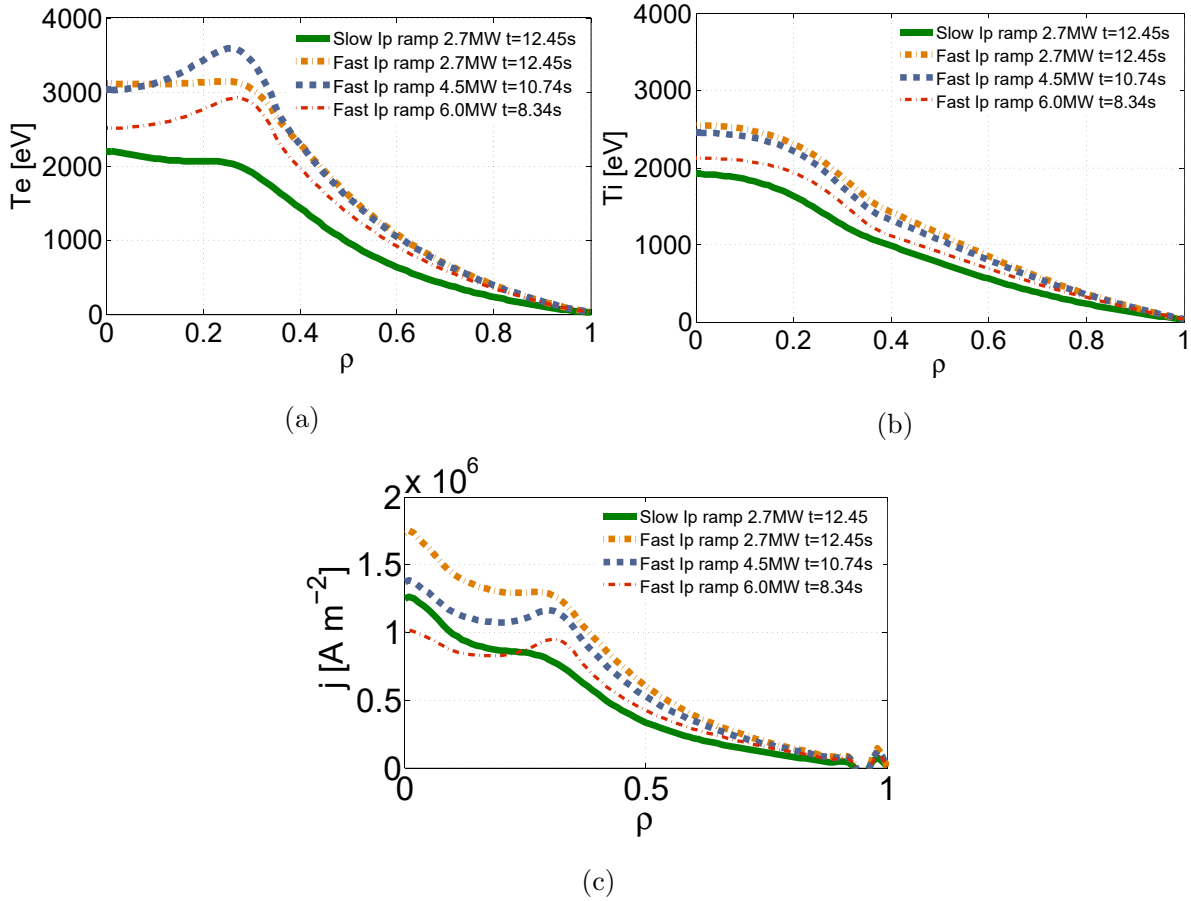

Figure 24. JT-60SA: (a) T_e profiles, (b) T_i profiles, (c) current density profiles prior to L-H transition.

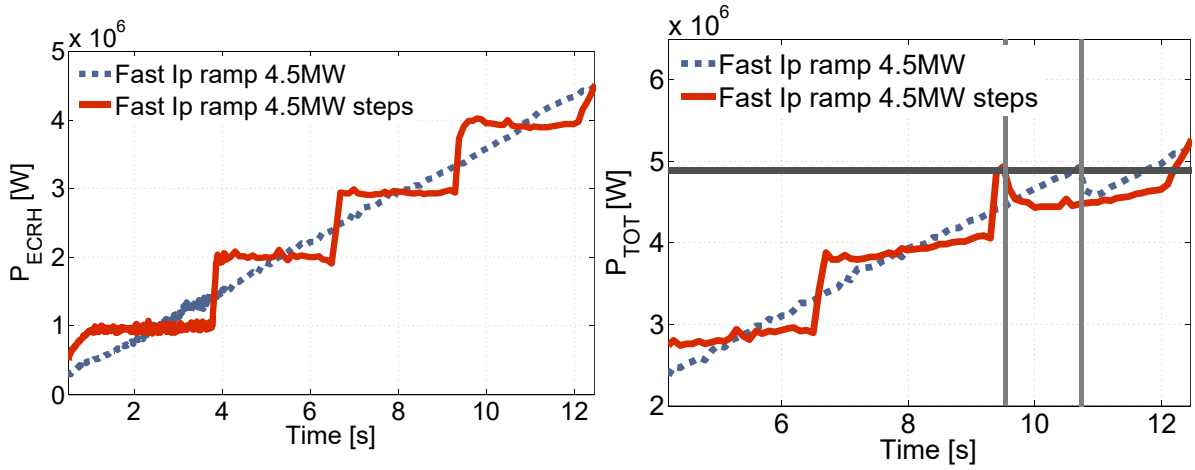

Figure 25. JT-60SA: (left) ECRH power injected, (right) total power (ECRH plus ohmic) and L-H transition threshold (horizontal gray line).

(right); for all cases we observe very small changes for the considered times, keeping in mind that the average density is almost constant between $t = 3$ s and $t = 12.45$ s (see figure 11).

As previously mentioned, the ECRH power injection needed to maintain the q profile above unity for the fast Ip ramp is higher than for the slow Ip ramp. In figure 22, we note that the q profile is marginally above one in the 4.5 MW case, and that it is completely above unity for an EC ramp of 6.0 MW. In these measurements, we also compare the slow Ip ramp case at 2.7 MW. Based on the above results, we conclude that increasing the current ramp-up rate has a strong impact on the amount of ECRH power needed to maintain the q profile above unity.

Little variation in the EC power deposition peak can be observed (see figure 23), and the power is well deposited around $\rho = 0.33$. The temperature and current density profiles

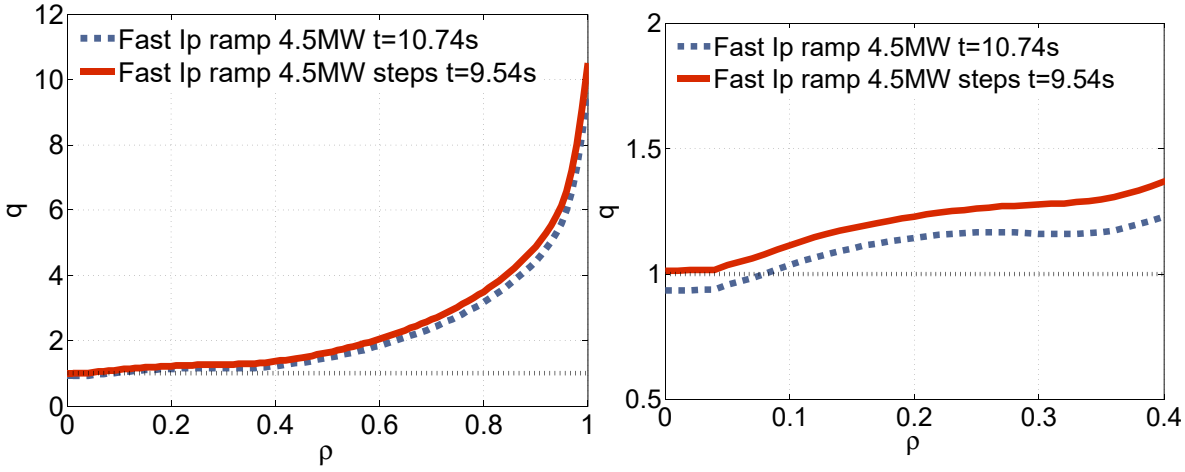

Figure 26. JT-60SA: (left) q profile, (right) zoom of q profile prior to L-H transition.

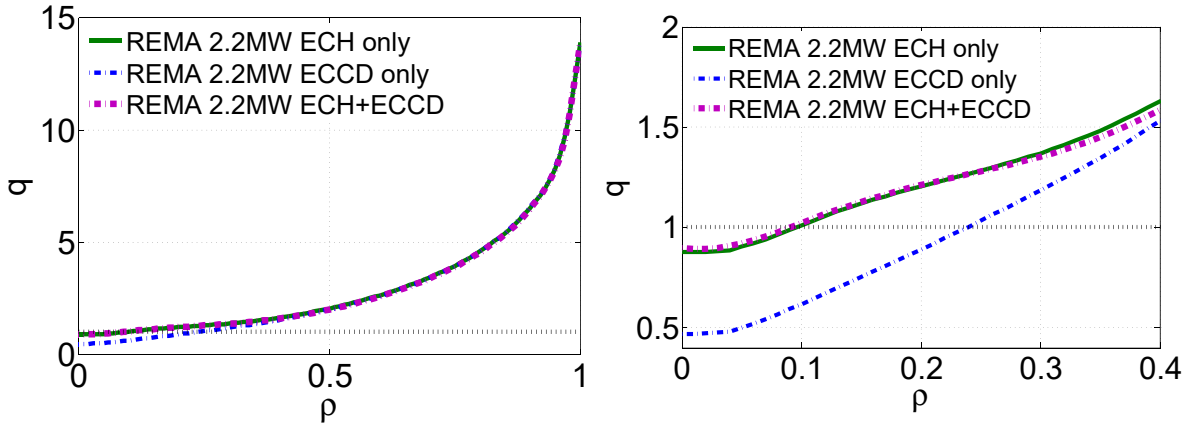

Figure 27. JT-60SA: (left) q profile at L-H transition, (right) core q profile at $t = 12.45$ s (L-H transition).

in figure 24 show that ohmic power is not negligible, the central T_e goes from near 2 keV for the slow Ip ramp to more than 3 keV for the fast Ip ramp, at the same level of EC power injection (2.7 MW). For a high power and fast Ip ramp, the T_e profile is hollow; this is reflected in a slightly reversed q profile (see figure 22 right, we observe a local minimum at $\rho \approx 0.34$ for fast Ip ramp at 4.5 MW and 6.0 MW of ECRH). For all cases, the observed temperature ratio is $T_i/T_e > 0.5$.

To compare our model with a more realistic EC power ramp, where each gyrotron is turned on one by one, we performed a simulation, taking as reference the fast Ip ramp with 4.5 MW. In figure 25 we plot both cases. At each step we increase the EC power by 1 MW. The L-H transition arrives early in the staircase scenario, at 9.54 s, compared to 10.74 s. The transition occurs at the same total power as the reference case, at 4.9 MW (see figure 25 right). In figure 26 we plot the q profiles prior to L-H transition. We observe that there is no significant change in their shape. We conclude that increasing the EC power by increments does not significantly affect the resulting q profile.

In the final part of this study we analyze the independent contribution of EC heating and EC current drive on q profile shaping. To this end, we artificially turn off the EC current drive and the EC heating in two different simulations, and compare the results to the standard simulation where the two sources coexist. We take into account the slow Ip ramp with an EC power ramp at 2.2 MW for $t = 12.45$ s (see figure 10). Based on figure 27, we can clearly observe that the EC current drive does not play a major role in safety factor profile shaping. Taking into account only the EC heating source (without current drive) the calculated q profile compares very well to the standard case. In fact, the electron temperature and the current density profile are not modified with EC current drive only (see figure 28). We observe in this last figure that only the EC heating source is needed to explain the changes in the T_e and

Table 1. Estimation of EC power needed.

	EC power rate	Turn on 1 MW gyrotron (25% loss) every	Total power needed (1MW gyrotrons)
Slow Ip	0.2 MW s^{-1}	3.75 s	3 MW (4 gyrotrons)
Fast Ip	0.4 MW s^{-1}	1.88 s	4 MW (6 gyrotrons)

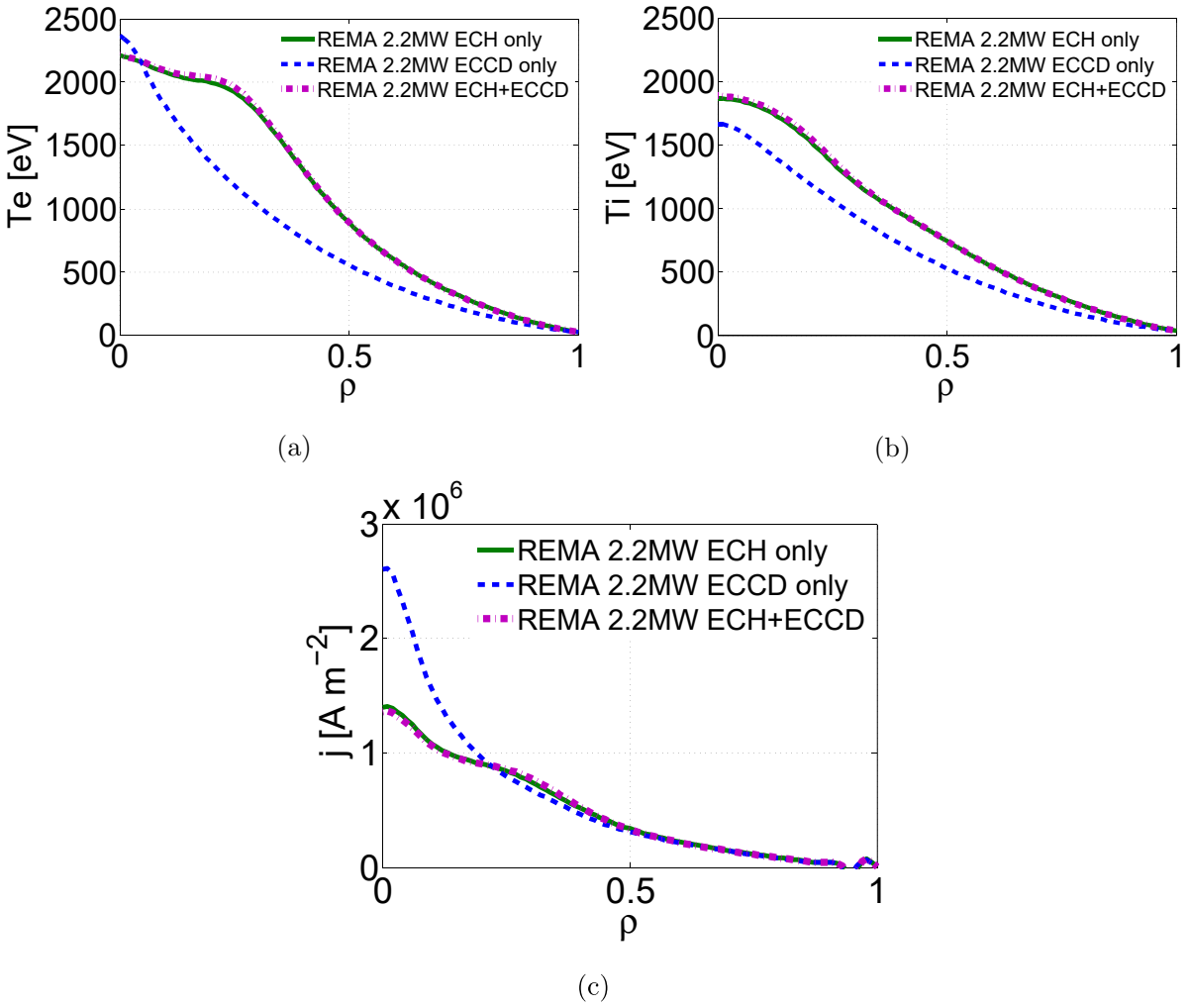

Figure 28. JT-60SA: (a) T_e profiles, (b) T_i profiles, (c) current density profiles at $t = 12.45$ s (L-H transition).

j profiles. Moreover, for these cases, the temperature ratio is found to be $T_i/T_e > 0.5$.

5. Conclusion

In this paper, modeling framework allowing the simulation of ECRH-assisted current ramp-ups has been validated, and was applied to the study of a JT-60SA hybrid #4-2 scenario ramp-up. In the validation exercise we use JET current ramp-up data, taking into account a pulse with MSE constrained equilibrium reconstruction. The MSE constraint allows us to better estimate the central safety factor profile evolution. Interpretative simulations using CRONOS (evolving only the current diffusion equation) show that neoclassical resistivity computations allow us to recover the experimental q profile evolution. A sensitivity study shows that uncertainties of edge electron temperature can play an important role in q profile. A change of 15% in the edge electron temperature induces changes of more than 10% in q profiles. On the other hand if Z_{eff} is substantially modified (for example taking decreasing/increasing linear profiles, as presented in figure 2) the changes in safety factor amount to only a few percent. The change in edge T_e is reflected directly in the neoclassical resistivity profile. For example if T_e at the plasma periphery decreases, the edge resistivity grows (by around the same percentage); this effect increases the current diffusion into the plasma, accelerating the drop of central q. Using the same JET data, we then ran predictive simulations (evolving the flux function ψ, T_e and T_i) to test two different turbulence transport model CDBM and TGLF. These simulations show that both models can accurately predict the safety factor. Nevertheless a drawback is detected with respect to the TGLF model. This models works if a boundary condition is imposed at $\rho = 0.9$; if the entire plasma radius is simulated with TGLF (boundary condition imposed at $\rho = 1$) the edge ion and electron temperatures are overestimated (i.e., a small edge temperature pedestal forms). For this reason, we selected CDBM as the turbulence model in the remainder of the study.

In the second validation exercise, we tested the ECRH ray-tracing and source power deposition code REMA, coupled with the CDBM turbulence model. With this aim, we utilized experimental data from a TCV flat-top phase where ECRH and NBI are both applied. In this case we evaluated two instants: the first where X2 and X3 EC waves are injected, and the second where we had X2 and NBI. The simulation results show that electron temperature profiles are well captured at the EC phase, and also when NBI is applied. On the other hand, ion temperature profiles are underestimated in both phases. This effect can be explained by the fact that CDBM computes a single thermal diffusivity which is applied to both T_e and T_i. CDBM solves the transport coefficient for the pressure $P = n_e(T_e + T_i)$ equation. In a case where T_e and T_i differ, the transport coefficient for the temperature profile with higher gradients is well computed. Therefore in our case, with $T_e > T_i$, higher temperature gradients are on the electron channel, and the CDBM prediction is accurate for T_e but underestimates T_i. As we are interested in ECRH assisted current ramp-ups where, in general, $T_e > T_i$, we conclude that the chosen modeling framework (REMA and CDBM) can be used, but with a certain degree of caution. In the remainder of this study, we verified the ratio $T_i/T_e > 0.5$ in order to limit T_i underpredictions. The big advantages of CDBM are its speed and its capacity to model all the plasma radii, up to $\rho = 1$.

With the previously defined modeling framework, we studied a JT-60SA hybrid #4-2 scenario current ramp-up. We show that a compromise between a q profile larger than unity and high central T_e imposes a radial power deposition close to $\rho = 0.33$. We recall that our main objective is to achieve a q profile above unity prior to L-H transition in scenario #4-2. Two current ramps are studied: a fast one, where the Ip plateau is reached at $t = 15$ s and a slow one, where the same plateau is reached at $t = 28.5$ s. For the fast current ramp we find that in order to achieve a q profile above unity we need an EC power ramp ranging from at least 0.16 MW at $t = 0.5$ s to 4.5 MW at $t = 12.45$ s. In this case, the L-H transition occurs at $t = 10.74$ s. For the slow Ip ramp, a lower ECRH is needed to achieve the same objective, i.e. a ramp from 0.16 MW at $t = 0.5$ s to 2.7 MW at $t = 12.45$ s. Here, the L-H transition occurs at $t = 12.45$ s. This example shows that increasing the current ramp-up rate strongly increases the need for ECRH to control the q profile prior to L-H transition. This requirement should be balanced with the benefits of a faster ramp-up for the overall scenario design.

A staircase increase of EC power does not significantly modify the resulting q profile. Based on these results, we can estimate roughly the time between every 1 MW gyrotron start-up and the number of gyrotrons needed to obtain the desired q profile. In the estimation we considered a loss of 25% in the transmission lines for each 1 MW gyrotron (see table 1).

Finally, in the last part of our study we show that q profile shaping is accomplished primarily by the EC heating source. We observe that the computed EC current drive has no effect on the safety factor profile.

Acknowledgments

The authors gratefully acknowledge members of the JT-60SA Integrated Project Team for data exchange and fruitful discussions.

This work has been carried out within the framework of the EUROfusion Consortium, and has received funding from the Euratom research and training programme 2014-2018 and 2019-2020, under Grant Agreement No. 633053. The views and opinions expressed herein do not necessarily reflect those of the European Commission.

ORCID iDs

J Morales https://orcid.org/0000-0002-3140-0504
J Garcia https://orcid.org/0000-0003-0900-5564
G Giruzzi https://orcid.org/0000-0001-9628-5968
C Piron https://orcid.org/0000-0002-4441-9781
M Vallar https://orcid.org/0000-0002-1792-6702

References

[1] Imbeaux F *et al* 2011 *Nucl. Fusion* **51** 083026
[2] Voitsekhovitch I *et al* 2010 *Plasma Phys. Control. Fusion* **52** 105011
[3] Wakatsuki T, Suzuki T, Hayashi N, Shiraishi J, Ide S and Takase Y 2015 *Plasma Phys. Control. Fusion* **57** 065005
[4] Barabaschi P, Kamada Y and Shirai H *et al* 2019 *Nucl. Fusion* **59** 112005
[5] Giruzzi G *et al* 2019 *Plasma Phys. Control. Fusion* **62** 014009
[6] Garcia J *et al* 2014 *Nucl. Fusion* **54** 093010
[7] Garzotti L *et al* 2018 *Nucl. Fusion* **58** 026029
[8] Itoh K, Yagi M, Itoh S-I, Fukuyama A and Azumi M 1993 *Plasma Phys. Control. Fusion* **35** 543
[9] Itoh K, Itoh S, Fukuyama A, Yagi M and Azumi M 1994 *Plasma Phys. Control. Fusion* **36** 279–306
[10] Honda M and Fukuyama A 2006 *Nucl. Fusion* **46** 580–93
[11] Staebler G, Kinsey J and Waltz R 2005 *Phys. Plasmas* **12** 102508
[12] Artaud J *et al* 2010 The cronos suite of codes for integrated tokamak modelling *Nucl. Fusion* **50** 043001
[13] JT-60SA Research Unit JT-60SA Research Plan 2018. Research Objectives and Strategy v4.0, Sept. (available at: www.jt60sa.org/pdfs/JT-60SA_Res_Plan.pdf)
[14] Brix M, Hawkes N, Boboc A, Drozdov V, Sharapov S and JET-EFDA Contributors 2008 *Rev. Sci. Instrum.* **79** 10F325
[15] Houlberg W, Shaing K-C, Hirshman S and Zarnstorff M 1997 *Phys. Plasmas* **4** 3230–42
[16] Fietz S *et al* 2013 *Nucl. Fusion* **53** 053004
[17] Waltz R, Candy J and Bravenec R 2017 *APS Meeting Abstracts*
[18] Hayashi N *et al* 2017 *Nucl. Fusion* **57** 126037
[19] Krivenski V, Fidone I, Giruzzi G, Granata G, Meyer R and Mazzucato E 1985 *Nucl. Fusion* **25** 127
[20] Goldston R, McCune D, Towner H, Davis S, Hawryluk R and Schmidt G 1981 *J. Comput. Phys.* **43** 61–78
[21] Pankin A, McCune D, Andre R, Bateman G and Kritz A 2004 *Comput. Phys. Commun.* **159** 157–84
[22] Pereverzev G V and Yushmanov P 2002 *ASTRA. Automated System for TRansport Analysis in a tokamak*
[23] Martin Y *et al* 2008 *J. Phys.: Conf. Series* **123** 012033